Front Propagation in Patterned Precipitation. 1. Simulation of a Migrating $Co(OH)_2$ Liesegang Pattern

M. Al-Ghoul[†,‡] and R. Sultan*[,†]

Department of Chemistry and Center for Advanced Mathematical Sciences, American University of Beirut, Beirut, Lebanon

Received: March 27, 2001; In Final Form: June 7, 2001

The model of Müller and Polezhaev for periodic precipitation is applied to a salt system that can dissolve in excess diffusing electrolyte due to complex formation. A typical example is the $Co(OH)_2$ Liesegang pattern from Co^{2+} and NH_4OH, which propagates due to band formation ahead and band dissolution at the tail of the stratum ($Co(OH)_2$ dissolves in excess ammonium hydroxide forming $Co(NH_3)_6^{2+}$). Diffusion profiles are constructed by plotting the computed distance of the last band (d_{lb}) and that of the first band (d_{fb}) versus time. The propagation is investigated under two main conditions: at fixed concentration of the inner electrolyte (X_0) while varying that of the outer electrolyte (Y_0), and the reverse (i.e., at fixed Y_0 while varying X_0). While in the first case, the propagation is faster at higher Y_0, the opposite trend is obtained when X_0 is varied, exactly reproducing the experimental observations in the literature on $Co(OH)_2$. A correlation close to linear is found between the dissolution and precipitation events. The advancing banded patterns are also displayed in a special map representation combining the diffusion profiles with the band contours. A special criterion is developed, delineating the situations where either a single pulse or a stratum of bands propagates.

1. Introduction

A Liesegang[1,2] pattern is a stratification of parallel precipitate bands obtained when two coprecipitate ions interdiffuse in a gel medium. A variety of systems yielding sparingly soluble salts exhibits this fascinating phenomenon in a wide collection of bibliographic sources built up over more than a hundred years. The dynamics of Liesegang banding is very rich and can be very complex, involving the coupling of diffusion and precipitation processes in a nonequilibrium regime. Despite this, most of the well-known Liesegang patterns are stationary, in the sense that the bands are "locked" in their positions once they are formed. In that context, Liesegang structures were viewed by Ross and co-workers[3] as an example of Turing[4] patterns. A small category of Liesegang systems is, however, dynamic, displaying a propagation of the whole pattern behind the diffusing electrolyte. This propagation is due to the dissolution of precipitate bands in excess electrolyte. Thus, in a vertical tube, new bands form at the bottom, and old ones dissolve at the top, yielding an apparently moving stratum of bands down the tube. A typical example of this class of periodic structures is the $Co(OH)_2$ system[5] from Co^{2+} and NH_4OH. The precipitate $Co(OH)_2$ dissolves in excess ammonium chloride[6] due to complexation of Co^{2+} with ammonia[7] (see the chemical reaction scheme in section 2). Thus the precipitation of $Co(OH)_2$ competes with its own dissolution in excess ammonium chloride, leading to this precipitation/dissolution scenario. A rich dynamics of this propagating pattern hence emerges, involving the velocities of front propagation, the correlation between the events at the top and the bottom of the tube, and even a chaotic oscillation of the total number of bands within the traveling zone.[5]

In the present paper we attempt to account for the behavior observed experimentally, by proposing a model for the system of chemical reactions involved. We then study the coupling of those precipitation/dissolution reactions to the diffusion of the aqueous species involved, using the model of Müller and Polezhaev.[8] The model incorporates both the nucleation of small particles (nuclei) and their subsequent growth into large particles as a concerted mechanism for precipitation. The aims of the present study may now be summarized as follows:

1. Predict the formation of the pattern of $Co(OH)_2$ bands and monitor its time evolution to demonstrate its advancement in space through precipitation and dissolution.

2. Study the effect of varying the concentration of NH_4OH (outer electrolyte) on the spatio-temporal evolution of the pattern, by obtaining the diffusion profiles and the plots of spatial precipitate distribution (bands).

3. Study the effect of varying the concentration of Co^{2+} (inner electrolyte) on the spatio-temporal evolution of the pattern, by obtaining the diffusion profiles and the plots of spatial precipitate distribution (bands).

4. Investigate the correlation between the dissolution and precipitation events at the two ends of the band stratum.

5. Compare the theoretical results with the experimental findings[5].

2. Model

Consider the following reaction of the precipitation of Co(II) hydroxide and its subsequent dissolution in excess ammonia:

$$Co^{2+}(aq) + 2NH_4OH(aq) \xrightarrow{k} 2NH_4^{+}(aq) + Co(OH)_2(s)$$

$$Co(OH)_2(s) + 6NH_4^{+}(aq) \xrightarrow{k'} Co(NH_3)_6^{2+}(aq) + 2H_2O(l) + 4H^{+}(aq)$$

By introducing a simplified reaction scheme incorporating both precipitation and dissolution (shown below), we adopt the model

[†] Department of Chemistry.
[‡] Center for Advanced Mathematical Sciences.

10.1021/jp011158o CCC: $20.00 © 2001 American Chemical Society
Published on Web 08/07/2001

of Müller and Polezhaev (MP)[8] for the analysis of the reaction−diffusion equations. The weakly soluble precipitate $Co(OH)_2$(s) is usually described by a continuous spatio-temporal particle size distribution function. However, in the MP model, two particle sizes, small and large, are used to characterize the precipitate.

Let $\tilde{\rho}$ denote the average density of solid salt in the form of small particles (called nuclei in ref 8), and ρ the average density of solid salt in the form of big particles. Let c be the concentration of the dissolved salt $Co(OH)_2$(aq). If c exceeds some critical value c_3, small particles (nuclei) nucleate in the salt solution with a rate of nucleation v_1. If c exceeds some other parameter c_2, nuclei are transformed into large particles at a rate v_3; otherwise, they dissolve at a rate v_2. Finally, if c exceeds a certain value c_1, large particles grow at a rate v_4.

2.1. Evolution Equations. We introduce the following variables

$$\mathrm{X} = \mathrm{Co}^{2+}(\mathrm{aq})$$

$$\mathrm{Y} = \mathrm{NH_4OH(aq)}$$

$$\mathrm{Z} = \mathrm{NH_4}^{+}(\mathrm{aq})$$

$$\mathrm{A} = \mathrm{Co(OH)_2(s)}$$

The above reaction scheme is reduced to a simpler form as follows:

$$\mathrm{X} + 2\mathrm{Y} \xrightarrow{k} 2\mathrm{Z} + \mathrm{A} \tag{1}$$

$$\mathrm{A} + 6\mathrm{Z} \xrightarrow{k'} \mathrm{P} \tag{2}$$

We assume that the dissolved salt of concentration c is different from the complex $Co(NH_3)_6^{2+}$(aq), called P in eq 2. The conservation equations for the electrolyte concentrations diffusing and reacting are given by

$$\frac{\partial X}{\partial t} = D_{\mathrm{X}}\nabla^2 X - kXY^2 \tag{3}$$

$$\frac{\partial Y}{\partial t} = D_{\mathrm{Y}}\nabla^2 Y - 2kXY^2 \tag{4}$$

where D_{X} and D_{Y} are diffusion coefficients of X and Y, respectively, ∇^2 is a one-dimensional Laplacian, and k is a precipitation rate constant. The addition of excess Z induces dissolution of the precipitate in the form of the complex $Co(NH_3)_6^{2+}$(aq). The evolution of Z is given by

$$\frac{\partial Z}{\partial t} = D_{\mathrm{Z}}\nabla^2 Z - 6k'Z^6\rho + 2kXY^2 \tag{5}$$

where D_{Z} is the diffusion coefficient of species Z and k' denotes the rate constant of dissolution.

The dynamics of the average particle sizes, $\tilde{\rho}$ and ρ, is given by

$$\frac{\partial \tilde{\rho}}{\partial t} = v_1(c) - [v_2(c) + v_3(c)]\tilde{\rho} \tag{6}$$

$$\frac{\partial \rho}{\partial t} = v_3(c)\tilde{\rho} + v_4(c)\rho - 6k'Z^6\rho \tag{7}$$

The concentration of dissolved salt, c, is given by

$$\frac{\partial c}{\partial t} = D_{\mathrm{c}}\nabla^2 c + kXY^2 - v_1(c) + v_2(c)\tilde{\rho} - v_4(c)\rho + 6k'Z^6\rho \tag{8}$$

where D_{c} is the diffusion coefficient of dissolved salt.

We still have to specify the explicit form of the rate function $v_i(c)$ to complete the description of the problem. It is shown[8] that the shape of the $v_i(c)$'s does not affect the qualitative appearance of the result. Therefore, we only assume that they are monotonic functions of c as follows:

$$v_1(c) = \alpha(c - c_3)\theta(c - c_3) \tag{9}$$

$$v_2(c) = \beta(c_2 - c)\theta(c_2 - c) \tag{10}$$

$$v_3(c) = \gamma(c - c_2)\theta(c - c_2) \tag{11}$$

$$v_4(c) = \delta(c - c_1)\theta(c - c_1) \tag{12}$$

where α, β, γ, and δ are rate constants and $\theta(x)$ is the Heaviside function.

2.2. Numerical Method. Equations 3−8 were solved numerically with the following initial conditions

$$X(t = 0, x) = X_0\theta(x - L/2)$$

$$Y(t = 0, x) = Y_0\theta(L/2 - x)$$

$$\tilde{\rho}(t = 0, x) = \rho(t = 0, x) = Z(t = 0, x) = c(t = 0, x) = 0$$

and the following no-flux boundary conditions

$$\mathbf{n}\cdot\nabla \mathrm{X}|_{x=L} = \mathbf{n}\cdot\nabla \mathrm{Y}|_{x=L} = \mathbf{n}\cdot\nabla \mathrm{Z}|_{x=L} = \mathbf{n}\cdot\nabla c|_{x=L} = 0$$

where x is the spatial independent variable and L is the length of the tube in which the reaction is taking place. The length L is partitioned into an equally spaced mesh of 400 grid points. Equations 3−8 are then discretized according to a second-order centered finite difference scheme to compute the Laplacians. The resulting ordinary differential equations are solved using Gear's method[9] for stiff-differential equations. We decreased the size of the mesh by increasing the number of grid points to 800 keeping the same length. The results did not change qualitatively. The number of bands and the spacing remained the same.

3. Results

The spatial distribution of the precipitate at a certain time t is given by the function $\rho(t)$. Figure 1 shows the time evolution of the average particle density ρ. We clearly see that the pattern of bands advances behind the NH_4OH front, by virtue of the dissolution of bands at the back and the formation of new ones at the front. This is equivalent to band dissolution at the top and band formation at the bottom in a vertical tube, resulting in the migration of the whole pattern down the tube. We now look at the diffusion profiles obtained by plotting the distance of the last band from the origin (d_{lb}) and that of the first band (d_{fb}) with time. (The origin is defined here as the junction between the two solutions: Co^{2+} (inner) and NH_4OH (outer).) The resulting curves are shown in Figure 2. The representation used is a contour profile-pattern map, highlighting the locations of the bands, together with a space−time plot obtained by drawing contour lines joining the edges of the first and the last bands (actually their locations x) at a specific time t. The white contour curves thus represent the plots of d_{lb} and d_{fb} versus time t. The correlation between the two distances d_{fb} and d_{lb} were shown experimentally[5] to be linear. We test our model by constructing such a correlation plot, obtained by plotting d_{lb} versus d_{fb}, as depicted in the inset of Figure 2. A clear correlation is seen to exist between the two variables (though not perfectly linear), generally in good agreement with the experimental result. The nonlinearity is attributed to the complexity of the problem

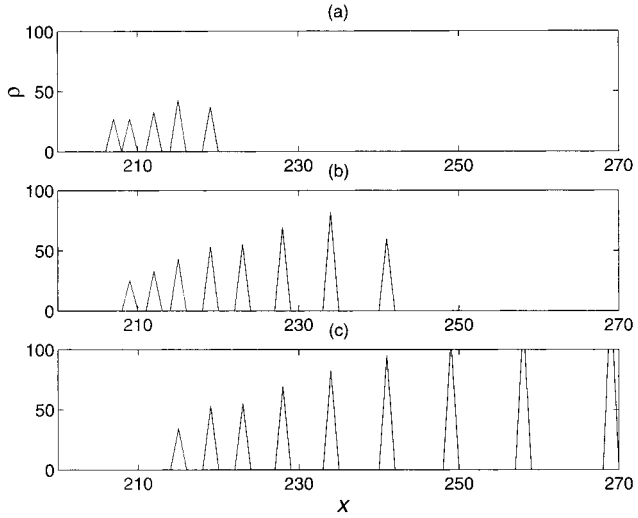

Figure 1. Time evolution of a propagating Liesegang pattern in 1D. The pattern advances by dissolution of old bands at the top of the tube (at the left here) and formation of new ones at the bottom (right). Model parameters: $X_0 = 10$; $Y_0 = 100$; $Z_0 = 0$; $\tilde{\rho} = 0$; $\rho = 0$. $k = 1.0 \times 10^{-5}$; $k' = 1.0 \times 10^{-4}$; $D_X = D_Y = D_c = 1.0 \times 10^{-5}$; $D_Z = 1.0 \times 10^{-2}$; $c_1 = 2.1$; $c_2 = c_3 = 3.0$; $\alpha = 0.02$; $\beta = 0.01$; $\gamma = 0.01$; $\delta = 0.002$. Key: (a) $t = 8 \times 10^4$; (b) $t = 35 \times 10^4$; (c) $t = 125 \times 10^4$.

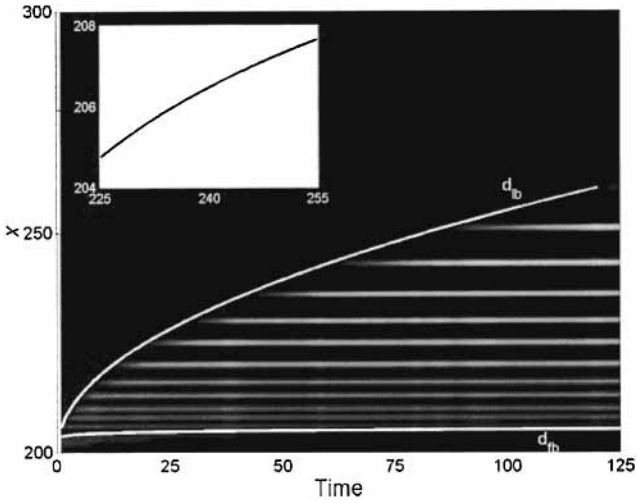

Figure 2. Diffusion profiles plotted as distance of last band (d_{lb}) and distance of first band (d_{fb}) versus time for the pattern shown in Figure 1. The bands are also shown in the location of their appearance. This representation is referred to as a contour profile/pattern map. Model parameters same as in Figure 1. The inset shows a correlation plot (d_{fb} versus d_{lb} at a given time). The correlation is close to linear.

and the existence of a large number of parameters. A similar nonlinear correlation was obtained upon varying the stoichiometric coefficient of the species Z in eq 2 and upon using equal values of the rate coefficients k and k'. Some additional notes on the properties of the model used and their impact on the obtained results are presented in the Discussion.

We now turn our attention to the effect of varying the concentration of either the outer or the inner electrolyte on pattern propagation. Figure 3 highlights the positions of the band strata at a fixed time, but at different initial concentrations of the outer electrolyte (Y_0). We see that the pattern propagates faster at a higher concentration of outer electrolyte, as indicated by a further location of the last band (at the same given time) when the initial concentration is higher. The corresponding diffusion profiles are depicted in Figure 4: the higher concentration curves lie above the lower concentration ones. Note that the latter plots could also be inferred from Figure 3, by joining

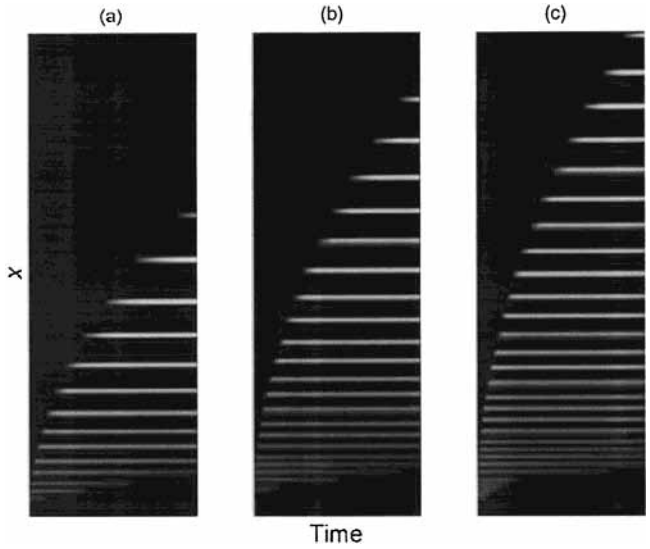

Figure 3. Profile-pattern maps of Liesegang bands at different initial concentrations of outer electrolyte (Y_0), computed all from $t = 0$ to $t = 125 \times 10^4$; $X_0 = 10$: (a) $Y_0 = 100$; (b) $Y_0 = 200$; (c) $Y_0 = 300$. The propagation is faster at higher Y_0, as indicated by a further migration of the whole stratum to the right (see notably the position of the last band).

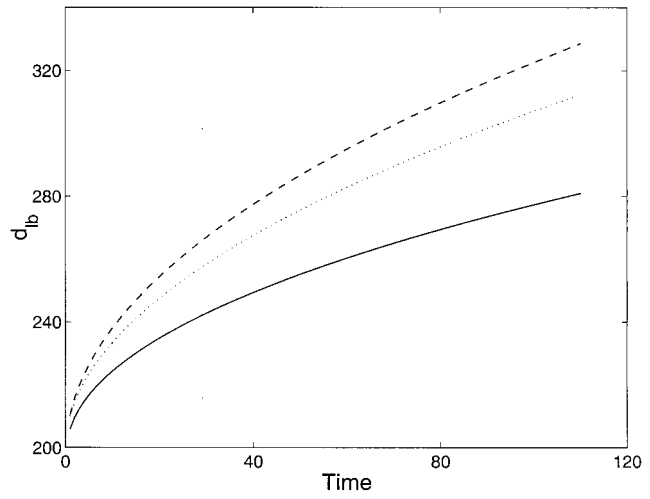

Figure 4. Diffusion profiles obtained from the plot of distance of last band (d_{lb}) versus time $t \times 10^4$, varying the concentration of outer electrolyte Y_0: $X_0 = 10$. Key: (solid curve) $Y_0 = 100$; (dotted curve) $Y_0 = 200$; (dashed curve) $Y_0 = 300$. The propagation is faster at higher Y_0 manifested here in the trend whereby the higher Y_0 curves lie above the lower Y_0 curves.

the band edges with a contour line (not shown) for the three different Y_0 concentrations. Next, we focus on varying the initial concentration of the inner electrolyte (X_0), a situation less frequently studied both experimentally and theoretically. Figure 5 shows diffusion profiles (distance of last band d_{lb} versus time t) at different values of X_0. We remark that exactly the opposite trend (to the one seen in Figure 4) is obtained, i.e., the lower concentration (X_0) curves lie above the high concentration ones. Thus the pattern advances faster in a lower X domain, reproducing the experimental result for $Co(OH)_2$[5] (with $X \equiv [Co^{2+}]$). The corresponding band patterns (plots of ρ versus space) are shown in Figure 6. The speed of propagation is higher at lower X_0, as indicated by the position of the last band at the fixed time reported. We also note that the band spacing at a given spatial position decreases as X_0 increases.

We now focus on the variation of the distance of first band (d_{fb}) with time. We investigate the effect of varying both the

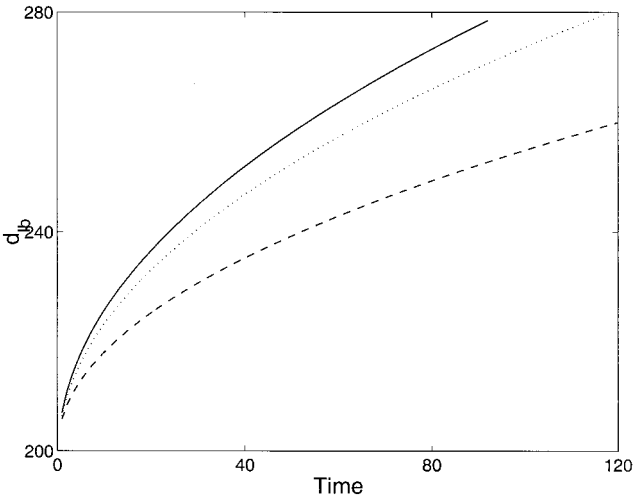

Figure 5. Diffusion profiles obtained from the plot of distance of last band (d_{lb}) versus time $t \times 10^4$, varying the concentration of inner electrolyte X_0: $Y_0 = 100$. Key: (solid curve) $X_0 = 9$; (dotted curve) $X_0 = 11$; (dashed curve) $X_0 = 17$. The opposite trend (to the one while varying Y_0) is obtained. The propagation is faster in a lower X_0 domain.

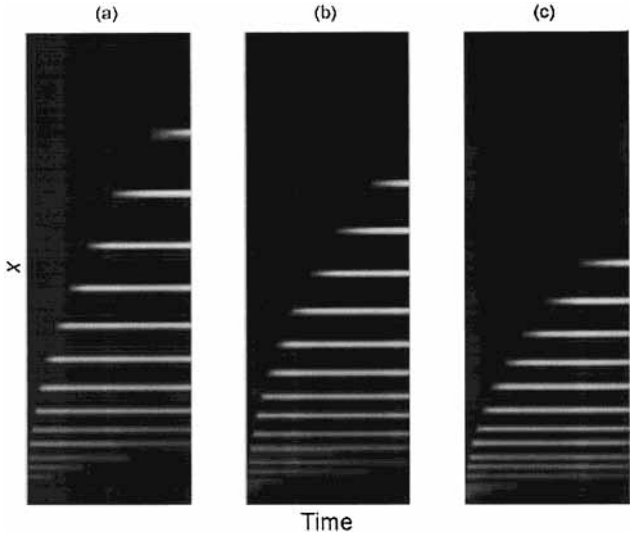

Figure 6. Profile-pattern maps of Liesegang bands varying X_0 (computed all from $t = 0$ to $t = 125 \times 10^4$): $Y_0 = 100$. Key: (a) $X_0 = 9$; (b) $X_0 = 11$; (c) $X_0 = 17$. The propagation is slower at higher X_0, indicated notably by a location of the last band which is closer to the interface (origin) as X_0 is increased.

inner and the outer electrolytes on the diffusion/dissolution profiles. Figure 7a shows plots of d_{fb} versus time at different initial concentrations of Y (Y_0); while Figure 7b displays the same plots varying the initial concentration of X (X_0). Exactly the same trends as for d_{lb} (seen in Figures 4 and 5) are obtained, thus clearly correlating the band dissolution and band formation events at both ends of the pattern, as suggested by the plot in the inset of Figure 2 and the experimental results of Nasreddine and Sultan.[5]

So far, we chose the constant c_2, the equilibrium threshold concentration of small particles, to be greater than c_1, the equilibrium threshold concentration of large particles. In other words, we are working in the case where small particles are more soluble than large particles, i.e., in the context of the Ostwald ripening instability[10,11] whereby small particles dissolve and diffuse then their masses are deposited on the large particles causing them to grow.[12] If we now reverse our choice of the parameters c_1 and c_2 in such a way that $c_2 = c_3 < c_1$,then we obtain a situation depicted in Figure 8, where a single band of

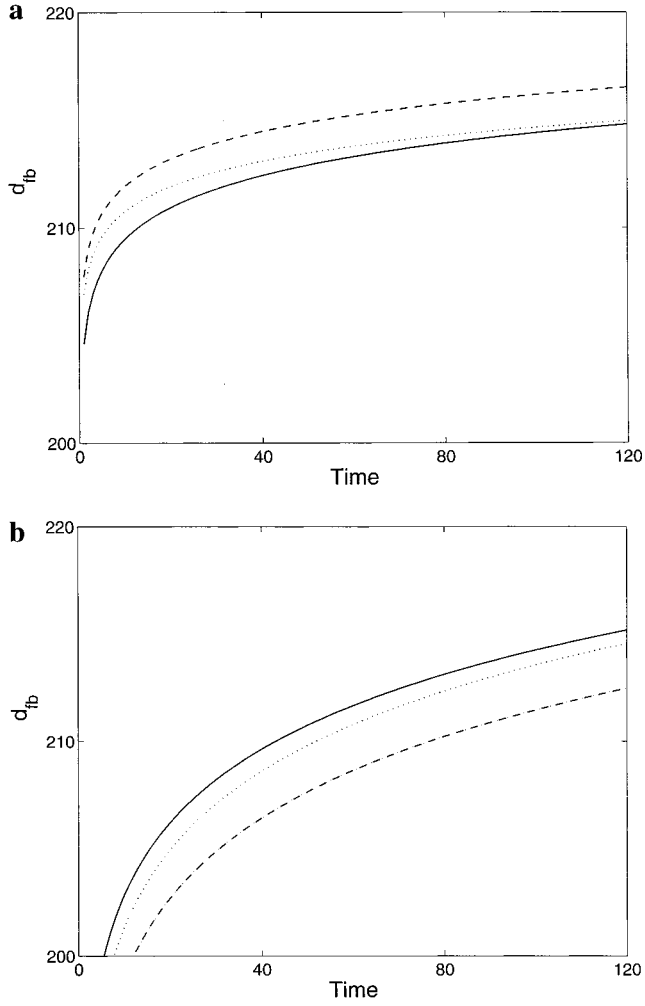

Figure 7. (a) Variation of distance of first band (d_{fb}) with time $t \times 10^4$, at three different Y_0 values: $X_0 = 10$. Key: (solid curve) $Y_0 = 200$; (dotted curve) $Y_0 = 300$; (dashed curve) $Y_0 = 400$. (b) Variation of distance of first band (d_{fb}) with time $t \times 10^4$, but now varying X_0: $Y_0 = 100$. Key: (solid curve) $X_0 = 9$; (dotted curve) $X_0 = 10$; (dashed curve) $X_0 = 11$. Exactly the same trend as for d_{lb} with the Y_0 and X_0 variations (shown in Figures 4 and 5 respectively) is obtained.

precipitate propagates and grows thicker in time, an observation reported in experimental studies on the $Cr(OH)_3$[13,14] and HgI_2[15,16] systems. This result is particularly interesting, as it could throw light on the system selectivity for single pulse versus band stratum propagation, and warrants further investigation. It could suggest ways of controlling the experimental conditions for the selection of either type of propagating pattern.

4. Discussion

The above study allowed a comparison of the properties of a migrating Liesegang pattern observed experimentally[5] with the dynamics of banded precipitation and dissolution conjectured using an existing theoretical model.[8] The effect of varying the initial concentrations of the outer and inner electrolytes reproduced and confirmed the experimental trends.

The formation of Liesegang bands characterizes the front propagation and pattern formation in reaction−diffusion systems where precipitation reactions are on the scene.[17] Theories of precipitate patterning are numerous and have been extensively reviewed.[2,17−19] The model of Müller and Polezhaev (MP),[8] applied here, is one of the most comprehensive theories, as it incorporates supersaturation, nucleation, and kinetics of particle growth as precipitation properties coupled to diffusion. Our

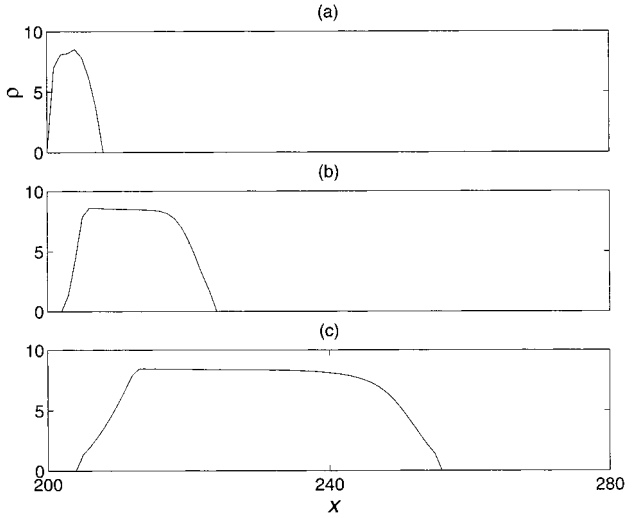

Figure 8. Propagation of a single precipitate band obtained in the case where $c_1 > c_2 = c_3$, i.e., the opposite situation to all the calculations performed so far. Parameters: $X_0 = 5$; $Y_0 = 20$; $Z_0 = 0$; $\tilde{\rho} = 0$; $\rho = 0$. $k = 1.0 \times 10^{-4}$; $k' = 1.0 \times 10^{-4}$; $D_X = D_Y = D_c = 1.0 \times 10^{-5}$; $D_Z = 1.0 \times 10^{-2}$; $c_1 = 2.1$; $c_2 = c_3 = 1.0$; $\alpha = 0.02$; $\beta = 0.01$; $\gamma = 0.01$; $\delta = 0.002$. Key: (a) $t = 2 \times 10^4$; (b) $t = 18 \times 10^4$; (c) $t = 125 \times 10^4$. Under this special condition, a single precipitate pulse propagates and grows thicker as seen in the time sequence a−c.

study adds to the previous model dissolution due to complex formation, a situation less frequently studied[6,20] theoretically. A profound comparison between the MP model used in this paper and other exisiting models is unfortunately not very feasible for two main reasons: (1) Almost all the work in the literature treats the precipitation reaction X + Y → A (where X and Y are coprecipitate ions and A is the precipitate) alone and does not consider the redissolution phenomenon due to complex ion formation. (2) All the recent theories focus mostly on the spacing law ($x_{n+1}/x_n = 1 + p$),[21−23] the width law ($w_n \sim x_n^{\alpha}$) (x_n and x_{n+1} are the locations of bands n and $n + 1$, respectively, and w_n is the width of the nth band.)[21,24] and the dependence of the spacing coefficient p on the initial concentrations of outer and inner electrolytes—the so-called Matalon−Packter law.[22] The main feature of interest in the present work is to simulate the propagation of the pattern and study the dissolution and precipitation events as they couple to diffusion. A discussion of the usefulness and feasibility of the MP model in addressing the problem of concern here is nevertheless relevant. The model is an extension of a class of theories that involve an intermediate species C in the precipitation reaction of the form: X + Y → ... C ... → A, where C could be a molecule, a droplet, or a colloid particle (here a small particle or nucleus). While in the original Ostwald theory[25] only the nucleation threshold is required, such schemes always involve two thresholds: one for nucleation and one for particle growth. On the other extreme, theories of postnucleation patterning,[26−28] based on an instability of an initial sol of different particle sizes, predict patterning in nucleation free systems. In MP, the model is enriched by considering three threshold values (c_1, c_2, and c_3), wherein a distinction is made between the transition to large particles ($c > c_2$) and the growth of those particles ($c > c_1$). At the same time, it preserves a simple form of the rate equations (9)−(11). However, it appears from our choice of parameters (see captions of Figures 1 and 8) that c_2 does not play a crucial role as it is taken to be equal to c_3 whether the latter is $\lessgtr c_1$. In other words, the dynamics could perhaps require only a transition from the formation of nuclei to their subsequent growth into particles, thus reducing to the two-threshold problem. When we used distinct values of c_2 and c_3, no convergence in the numerical calculation could be attained. The problem hence warrants further exploration in that direction. Note that nucleation was yet differentiated from the dissolution of the nuclei or their transition into large particles by choosing α to double $\beta = \gamma$. Note further that the case $c_2 = c_3$ is in conformity with the situation encountered in the original MP paper. Furthermore, in the present treatment, no constraint was imposed on the redissolution of the precipitate via reaction 2 except a control of the rate parameter k' (see eqs 7 and 8) for the sake of simplicity; i.e., no stepwise threshold values were involved in reaction 2. This latter condition constitutes the main variant of the model. Thus we see that so many parameters enter in that complex dynamics that a wide variety of modifications can be introduced and tested. A correction for the nonlinear correlation (section 3, inset of Figure 2) could perhaps be achieved via a careful navigation through the ranges of the diverse parameters.

In the modeling of a geochemical reaction scheme, dissolution was introduced in a study[20] based on the Ostwald cycle[25] to simulate the dissolution of pyrite (an iron sulfide mineral) by oxygen-rich water infiltrating through the rock medium. The subsequent deposition of goethite (an iron oxide mineral) behind the pyrite dissolution front ranged from steady pulse to "wiggle" structure to Liesegang bands as the nucleation rate parameter was varied.

In a following paper,[29] we investigate the influence of an applied constant electric field on the dynamics of pattern formation and propagation. The presence of the field was shown[30] to strongly alter the dynamics in the $Co(OH)_2$ system and modify the morphology of the bands. An electric field was also shown to strongly control the propagation of a single $Cr(OH)_3$ precipitate ring (like the one obtained here) in a two-dimensional gel medium.[14] In the theoretical study currently under inquiry, we also attempt to model the kinetics of that latter system. A variety of phenomena and diversity in structure are therefore expected to emerge.

Acknowledgment. This work was supported by a University Research Board (URB) grant, American University of Beirut.

References and Notes

(1) Liesegang, R. E. Lieseg. Phot. Archiv. **1896**, *21*, 221. Liesegang, R. E. *Naturewiss. Wochenschr*. **1896**, *11*, 353.

(2) Henisch, H. K. *Crystals in Gels and Liesegang Rings*; Cambridge University Press: Cambridge, U.K., 1988.

(3) Ross, J.; Arkin, A. P.; Müller, S. C. *J. Phys. Chem.* **1995**, *99*, 10417.

(4) Turing, A. M. *Philos. Trans. R. Soc. (London)* **1952**, *B237*, 37.

(5) Nasreddine, V.; Sultan, R. *J. Phys. Chem.* **1999**, *103*, 2934.

(6) Ostwald, Wo. *Kolloid Z.* **1925**, *36*, 380.

(7) Lloyd, F. E.; Moravek, V. *Plant Physiol.* **1928**, *3*, 101.

(8) Müller, S. C.; Polezhaev, A. A. *Chaos* **1994**, *4*, 631.

(9) Kahaner, D.; Moler, C.; Nash, S. *Numerical Methods and Software*; Prentice Hall: Englewood Cliffs, NJ, 1989.

(10) Liesegang R. *Z. Phys. Chem. (Leipzig)*, **1911**, *75*, 374.

(11) Lifshitz I. M., Slyozov V. V.: *J. Phys. Chem. Solids* **1961**, *19*, 35.

(12) Chernavskii, D. S.; Polezhaev, A. A.; Müller, S. C. *Physica D* **1991**, *54*, 160.

(13) Zrínyi, M.; Gálfi, L.; Smidróczki, É.; Rácz, Z.; Horkay, F. *J. Phys. Chem.* **1991**, *95*, 1618.

(14) Sultan, R.; Panjarian, Sh. *Physica D* **2001**, *157*, 243.

(15) Das, I.; Pushkarna, A.; Argawal, N. R. *J. Phys. Chem.* **1989**, *93*, 7269.

(16) Das, I.; Pushkarna, A.; Bhattacharjee, A. *J. Phys. Chem.* **1991**, *95*, 3866.

(17) Droz, M. *Lect. Notes Phys.* **1999**, *519*, 211.

(18) Stern, K. H. *Chem. Rev.* **1954**, *54*, 79. *A Bibliography of Liesegang Rings*, 2nd ed.; Government Printing Office; Washington, DC, 1967.

(19) Henisch, H. K. *Periodic Precipitation*; Pergamon Press: Oxford, U.K., 1991.
(20) Sultan, R.; Ortoleva, P.; DePasquale, F.; Tartaglia P. *Earth-Sci. Rev.* **1990**, *29*, 163.
(21) Dee, G. T. *Phys. Rev. Lett.* **1986**, *57*, 275.
(22) Antal, T.; Droz, M.; Magnin, J.; Rácz, Z.; Zrínyi, M. *J. Chem. Phys.* **1998**, *109*, 9479.
(23) Chopard, B.; Droz, M.; Magnin, J.; Rácz, Z.; Zrínyi, M. *J. Phys. Chem.* **1999**, *103*, 1432.
(24) Droz, M.; Magnin, J.; Zrínyi, M. *J. Chem. Phys.* **1999**, *110*, 9618.
(25) Ostwald, Wi. *Verwandtschaftslehre*; Lehrbuch der Allgemeinen Chemie; Engelmann: Leipzig, 1896−1902; 2. Aufl., Band 2, 2. Teil, p 778.
(26) Flicker, M.; Ross, J. *J. Chem. Phys.* **1974**, *60*, 3458.
(27) Feinn, D.; Scalf, W.; Ortoleva, P.; Schmidt, S.; Wolff, M. *J. Chem. Phys.* **1978**, *69*, 27.
(28) Venzl, G. *J. Chem. Phys.* **1986**, *85*, 1996.
(29) Al-Ghoul, M.; Sultan, R. Manuscript in preparation.
(30) Sultan R.; Halabieh, R. *Chem. Phys. Lett.* **2000**, *232*, 231.